Behavioural Brain Research 397 (2021) 112950

Contents lists available at ScienceDirect

Behavioural Brain Research

journal homepage: www.elsevier.com/locate/bbr

Implicit associative learning relates to basal ganglia gray matter microstructure in young and older adults

Corinna Y. Franco [a,*], Jessica R. Petok [b], Jason Langley [c], Xiaoping Hu [c,d], Ilana J. Bennett [a]

[a] Department of Psychology, University of California, Riverside, 900 University Avenue, Riverside, CA 92521, USA
[b] Department of Psychology, St. Olaf College, 1520 St. Olaf Avenue, Northfield, MN 55057, USA
[c] Center for Advanced Neuroimaging, University of California, Riverside, 900 University Avenue, Riverside, CA 92521, USA
[d] Department of Bioengineering, University of California, Riverside, 900 University Avenue, Riverside, CA 92521, USA

ARTICLE INFO

Keywords:
Implicit associative learning
Diffusion imaging
Basal ganglia
Hippocampus
Aging

ABSTRACT

Older adults are impaired at implicit associative learning (IAL), or the learning of relationships between stimuli in the environment without conscious awareness. These age effects have been attributed to differential engagement of the basal ganglia (e.g. caudate, globus pallidus) and hippocampus throughout learning. However, no studies have examined gray matter diffusion relations with IAL, which can reveal microstructural properties that vary with age and contribute to learning. In this study, young (18–29 years) and older (65–87 years) adults completed the Triplet Learning Task, in which participants implicitly learn that the location of cues predict the target location on some trials (high frequency triplets). Diffusion imaging was also acquired and multi-compartment diffusion metrics were calculated using neurite orientation dispersion and density imaging (NODDI). As expected, results revealed age deficits in IAL (smaller differences in performance to high versus low frequency triplets in the late learning stage) and age-related differences in basal ganglia and hippocampus free, hindered, and restricted diffusion. Significant correlations were seen between restricted caudate diffusion and early IAL and between hindered globus pallidus diffusion and late IAL, which were not moderated by age group. These findings indicate that individual differences in basal ganglia, but not hippocampal, gray matter microstructure contribute to learning, independent of age, further supporting basal ganglia involvement in IAL.

1. Introduction

Implicit associative learning (IAL) refers to the acquisition of relationships between events in the environment without explicit awareness [1]. Crucial throughout the lifespan, IAL supports the acquisition of language during childhood via the formation of associations between phonemes that produce words, as well as the learning of relationships between important cues and outcomes during social interactions and technological adaptation [2–5]. The Triplet Learning Task (TLT) is one way to assess IAL in the laboratory [6]. On each trial, or "triplet", participants respond to the location of a target that is preceded by two cues. Unbeknownst to participants, cue locations predict the target location on some trials (high frequency, HF) but not others (low frequency, LF). IAL is calculated as better accuracy or reaction time performance on HF compared to LF trials. Behavioral studies have reported reduced IAL in older versus younger adults, with larger age group differences in later stages of learning [7,5,6,8].

IAL performance, and age-related deficits therein, may be attributed to differential engagement of its neural correlates over the course of learning. For instance, we previously used functional magnetic resonance imaging (fMRI) to show that better late stage IAL was associated with learning-related activity (HF triplets > LF triplets) in bilateral caudate for young adults and in the hippocampus for older adults [9]. In a complementary study using diffusion tensor imaging (DTI), we showed positive relationships between early stage IAL and integrity of white matter tracts emanating from both the caudate and hippocampus in young and older adults, whereas late stage IAL was only related to caudate tract integrity in young adults but to caudate and hippocampus tract integrity in older adults [10]. Studies reporting no age group differences in the neural substrates of IAL often do not disaggregate results by learning stage. For example, one study using quantitative susceptibility mapping (QSM) found that iron concentration in caudate and globus pallidus positively correlated with overall IAL in both young and older adults [11]. As such, although there is converging evidence of

* Corresponding author.
E-mail address: cfran014@ucr.edu (C.Y. Franco).

https://doi.org/10.1016/j.bbr.2020.112950
Received 15 July 2020; Received in revised form 11 September 2020; Accepted 26 September 2020
Available online 2 October 2020

basal ganglia (caudate, globus pallidus) and hippocampal involvement throughout learning, a more comprehensive examination of relationships between learning and these neural substrates as a function of learning stage and aging is warranted, which is the focus of our current study.

A novel imaging approach to assess the microstructural properties of these gray matter structures is Neurite Orientation Dispersion and Density Imaging (NODDI). Using diffusion imaging data, NODDI separates the total diffusion signal into tissue and non-tissue sources, or compartments [12]. This multi-compartment approach provides separate measures of restricted (modeled as sticks), hindered (modeled as the dispersion of sticks), and free (modeled as an isotropic sphere) diffusion that are thought to reflect intracellular (e.g. neurite density), extracellular (e.g. dendritic arborization), and non-cellular (e.g. cerebrospinal fluid) sources of diffusion, respectively [12–15]. In this way, NODDI accounts for contamination of free diffusion in its other diffusion metrics, which may be prevalent in regions close to the ventricles (caudate, hippocampus) and in the aging brain [16].

Previous NODDI studies have reported age-related differences in microstructure of the hippocampus, seen as increases in free, hindered, and restricted diffusion [15,17–19] and select basal ganglia structures, seen as decreases in striatal (particularly caudate) hindered diffusion [15,20]. Researchers have interpreted these findings as older adults exhibiting differences in dendritic complexity in these regions compared to younger adults, although other neurobiological changes could be involved (e.g. iron accumulation, dendritic (de)arborization, vascular changes, and cell shrinkage) [21,22]. However, age-related differences in diffusion in other basal ganglia regions (e.g. globus pallidus, nucleus accumbens) have thus far been overlooked, and more importantly, no diffusion imaging studies have related gray matter microstructure to IAL or assessed age differences in these relationships.

To address these gaps in the literature, we had young and older adults perform a version of the TLT and undergo diffusion imaging. We aimed to examine (1) age group differences in IAL as a function of learning stage, (2) age group differences in basal ganglia (caudate, putamen, nucleus accumbens, globus pallidus) and whole hippocampus gray matter microstructure using NODDI, (3) relationships between early and late IAL and these neural substrates separately in each age group, and (4) whether these diffusion-learning relationships were moderated by age. Due to the influence of iron content (measured with R_2*) on diffusion metrics [23] and its accumulation over the lifespan in the basal ganglia [24,25], iron was treated as a variable of no interest in all diffusion analyses. We expected to replicate prior work finding age deficits in IAL, particularly in late learning, as well as increased diffusion in the hippocampus and decreased diffusion in striatum (caudate, putamen) in older adults compared to young adults, being the first to examine these effects in other basal ganglia structures (globus pallidum, nucleus accumbens) [15,17,18,20,19]. Based on the findings from other neuroimaging approaches, we further expected that better early stage IAL would relate to lower diffusion in the basal ganglia and hippocampus in both young and older adults, whereas late stage IAL would relate to lower diffusion in the basal ganglia in young adults and the basal ganglia and hippocampus in older adults, indicating a significant age group moderation of late learning-diffusion relationships.

2. Methods

2.1. Participants

Forty young (20.94 ± 2.11 years old, range = 18–29 years) and thirty older adults (73.06 ± 6.59 years old, range = 65–87 years) were recruited from the University of California, Riverside undergraduate research pool and surrounding communities, respectively. Prior to enrollment in the study, potential participants were screened over the phone for normal global cognition (> 17 on a subset of the Montreal Cognitive Assessment (MoCA) adapted for phone screening [26]), history of neurological conditions that could influence their performance (e.g. depression, stroke), and to ensure they could be scanned safely (e.g. pregnancy, claustrophobia, having metal inside the body). After enrollment in the study, seven participants were excluded from final analyses due to poor TLT performance (Accuracy [ACC] below two standard deviations from the young or older adult sample means respectively [approximately 50 %]; 2 young, 3 older), incomplete TLT data due to attrition (1 young), researcher error (1 young), or file corruption (1 older). The final sample consisted of 36 young (20.91 ± 2.19 years old, range = 18–29 years) and 26 older adults (72.82 ± 6.53 years old, range = 65–87 years) (see Table 1). All participants gave informed consent and received either course credit or monetary compensation for participation.

2.2. Procedure

Participants completed two separate 75-minute testing sessions approximately one week apart. During the first testing session, a high-resolution structural scan and a multi-echo gradient recalled echo (GRE) sequence were acquired. During the second testing session participants performed eight sessions of the TLT. To maximize scan time, sessions 1–3 (early stage) and 6–8 (late stage) were completed during functional scans (only the behavioral data will be reported here) and sessions 4–5 during diffusion scans. Immediately after scanning, participants were given the TLT recognition task and a post-test interview.

2.3. Triplet learning task

This version of the TLT was adapted from previous behavioral [6] and neuroimaging [9] studies. During this task, participants viewed four empty circles lined horizontally on a screen. Each trial consisted of a "triplet" of events in which one circle filled in red (cue 1; 150 ms), then a second filled in red (cue 2; 150 ms), and then a third circle filled in green (target; 800 ms). Triplet events were separated by a 150 ms inter-stimulus-interval, with a 600 ms inter-trial interval between triplets (total trial time was 2000 ms). Participants were instructed to passively view the red cues and respond quickly and accurately to the location of the green target using one of four button responses that corresponded to each of the four circle locations. Participants held one MR-compatible button box in each hand, each with separate buttons under their index and middle fingers. ACC and reaction times (RT) were collected for all trials.

Unbeknownst to participants, some triplets occurred with greater frequency and contained cues which predicted target locations (high-frequency, HF), while others occurred with lower frequency and were not predictive (low-frequency, LF). To optimize learning and remove triplet compositions occurring at other frequencies, HF triplets involved both first-order and second-order structure, meaning that the location of the first and second cue predicted the location of the target. As such, unlike other TLT versions [6], this task focused on the manipulation of

Table 1
Demographic characteristics of final sample.

	Young	Older
Sample size	36	26
Age (in years)		
Mean ± SD	20.91 ± 2.19	72.82 ± 6.53
Range	18 - 29	65 - 87
Gender (% of sample)		
Female	24 (66.67 %)	11 (42.31 %)
Male	12 (33.33 %)	15 (57.69 %)
Level of Education (in years)		
Mean ± SD	13.86 ± 1.33	15.96 ± 3.62
MoCA		
Mean ± SD	27.44 ± 1.40	27.19 ± 1.86
Range	24 - 29	23 - 30

Note. SD = standard deviation and MoCa = Montreal Cognitive Assessment.

joint (overall triplet frequency) but not conditional (within triplet statistical relationships) probability, which may have led to greater salience of both HF and LF triplets for young and older adults as well as more favorable learning for older adults who may otherwise struggle learning complex sequences.

Participants completed eight sessions of the task, each composed of four blocks of 32 triplets (1024 triplets total). For each block, four unique HF triplets were presented 6 times (24 H F triplets total) and eight unique LF triplets were presented once, forming a 3:1 ratio of HF (75 % frequency) to LF (25 % frequency) triplets. Triplets were counterbalanced to ensure that cues and targets occurred in each location equally often. Trials in every block were randomized, as well. Within a session, each block was separated by a 10 s break, during which "rest now" was presented in black text on a white screen. Sessions were separated by a break during which researchers manually restarted the task. Each session lasted approximately 5 min, with a total test time of approximately 47 min.

2.3.1. Recognition tests

Participants completed a recognition test outside the scanner after completing the full TLT. On each trial, they viewed a single triplet using the same stimuli and timing as in the TLT. They were instructed to indicate whether the triplet occurred "frequently", "infrequently", or "not at all" during the TLT using one of three button responses. The four unique HF triplets, eight unique LF triplets, and eight triplets that were not a part of the main study (no frequency, NF) were presented. NF triplets included those in which the first cue and target occurred in the same location (trills; e.g. 232, 434, where the numbers refer to the location of the three triplet events from the farthest left [1] to farthest right [4] circle) and those in which all triplet events occurred in the same location (repetitions; e.g. 333, 444).

After the recognition task, participants completed an interview to further ascertain explicit awareness. Interview questions were acquired verbatim from J. H. Howard et al. [6] and included the following: (1) "What strategy did you use to improve your speed and accuracy in the experiment?", (2) "Did you notice any relationship between either of the first two lights and the third light?", (3) "Did all the lights turn on equally often, or did some lights come on more often than others?", and (4) "In fact, there was a relationship between the first two lights and the third. What do you think it was for the first light? What about the second light?". Two young participants were dropped from recognition analyses only due to missing data, but their interviews were reviewed to ensure they showed no explicit awareness.

2.3.2. Calculating implicit associative learning (IAL) scores

Implicit associative learning (IAL) scores were calculated for each participant using behavioral data from the first three (1–3) and last three (6–8) sessions of the TLT that were completed during fMRI acquisition. The functional scans generated an artifact that was recorded as the same incorrect button response on every sixth and seventh trial. These trials were excluded prior to calculating IAL scores. Because the artifact occurred systematically and throughout the task, it had minimal impact on these IAL scores.

Mean accuracy and median reaction time on correct trials were calculated separately for HF and LF triplets for each block, and then averaged across blocks within each session. Mean of median reaction times for HF and LF triplets were then log-transformed to control for general slowing in age and separately averaged across sessions 1–3 (early IAL) and sessions 6–8 (late IAL) [27,28]. For correlation analyses, the averages of these log-transformed HF and LF mean of median RTs were subsequently subtracted from each other and multiplied by -1 to acquire measures of early and late IAL for which larger positive scores indicate better learning.

2.4. MRI scanning protocol

Imaging data were acquired with a 3-T Siemens Prisma magnetic resonance imaging (MRI; Siemens Healthineers, Malvern, PA) scanner using a 32-channel receive-only head coil at the Center for Advanced Neuroimaging at University of California, Riverside. A mirror attached to the head coil allowed participants to view the stimuli presented on a screen behind the MRI during the scan. Head movement was minimized by placing fitted padding around the head of each participant.

A single high-resolution structural image (magnetization-prepared rapid gradient-echo sequence, MP-RAGE) was acquired with the following parameters: echo time (TE)/repetition time (TR) = 2.72/2400 ms, 208 axial slices, voxel size = $0.8 \times 0.8 \times 0.8$ mm^3, and a Generalized Autocalibrating Partially Parallel Acquisitions (GRAPPA) acceleration factor of 2 [29].

Multiecho data derived from a 12-echo 3D GRE sequence were acquired with the following parameters: TE/ΔTE/TR = 4/3/40 ms, FOV = 192 mm × 224 mm, matrix size = $192 \times 224 \times 96$, slice thickness = 1.7 mm, and GRAPPA acceleration factor = 2. Magnitude images were obtained for calculation of R_2* values, which is a measure sensitive to iron concentration.

DTI data were acquired with a diffusion-weighted echo-planar imaging (EPI) sequence with the following parameters: TE/TR = 102/3500 ms, FOV = 212×182 mm, matrix size of 128×110, voxel size = $1.7 \times 1.7 \times 1.7$ mm^3, 64 axial slices, and multiband acceleration factor = 4. A second DTI scan was acquired with phase-encoding directions of opposite polarity for correction of susceptibility distortions [30]. For each DTI acquisition, bipolar diffusion encoding gradients (b = 1500 and 3000 s/mm^2) were applied in 64 directions, with six images having no diffusion weighting (b = 0; 12 total).

2.5. Regions of interest segmentation

Bilateral caudate, putamen, nucleus accumbens, and globus pallidus were automatically segmented on each participant's MP-RAGE using FSL's Integrated Registration and Segmentation Tool (FIRST; [31,32]), as illustrated in Fig. 1. Default settings were used for all regions except the hippocampus, where an additional flag specified a three-stage affine registration [33]. FIRST segmentations were based on observed intensities in each participants' MP-RAGE that were fit to the most probable surface meshes derived from shape and appearance models that were initially manually segmented and provided by the Center for Morphometric Analysis (CMA), MGH, Boston. A tissue-based classification was used to correct for overlap in boundary voxels. All segmented structures were aligned to diffusion images using a rigid body transformation (degrees of freedom [DOF] = 6) between the participants' MP-RAGE and their susceptibility distortion corrected DTI b = 0 image. All segmented structures were also aligned to R_2* maps using a transformation (DOF = 6) between each participants' MP-RAGE and the magnitude from the first echo of the 12-echo GRE acquisition. Aligned segmented structures were then binarized to create bilateral ROI masks.

All segmentations in structural space and mask alignments in diffusion and R_2* space were visually inspected to ensure accurate region capture. The latter revealed eight participants with misalignments (>1 voxel displacement) in diffusion space for the caudate, four of which were due to underestimation of the caudate in their initial FIRST segmentation and one of which did not accurately align caudate segmentations from MP-RAGE to diffusion space. For these five participants, the misalignments were corrected by rerunning the FIRST segmentation using the following adjustments: (1) linearly aligning each participant's MP-RAGE to a whole brain instead of a subcortical mask (the standard is a subcortical mask), (2) using the maximum number (336) of modes of variation for fitting (the standard number of modes for caudate is 40), and (3) using thalamus as a reference structure for intensity normalization (the standard uses the interior of the structure for intensity normalization). For the remaining three participants, misalignments for

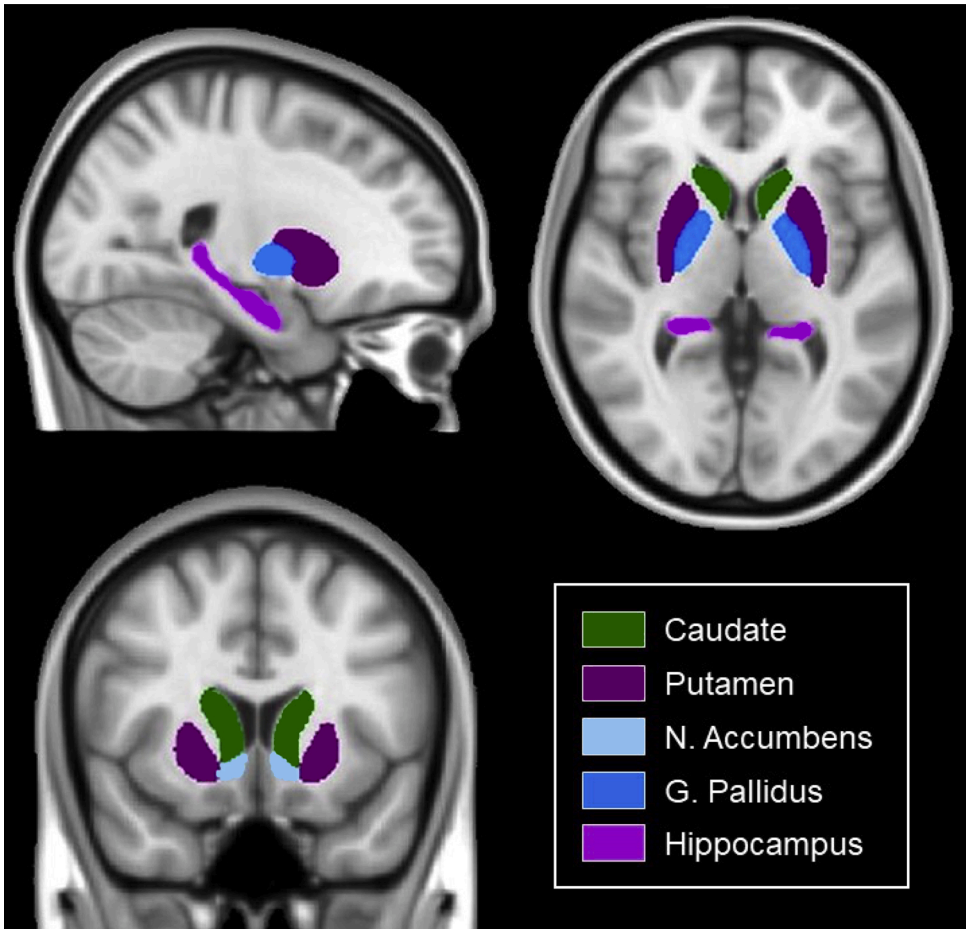

Fig. 1. Regions of interest. For illustration, bilateral caudate, putamen, nucleus accumbens, globus pallidus, and hippocampus were automatically segmented on a standard image (MNI 125 1 mm^3) using FSL's Integrated Registration and Segmentation Tool (FIRST).

caudate in diffusion space could not be fixed using these corrections and they were dropped from caudate analyses (3 young). Three participants also exhibited hippocampus segmentation issues in diffusion space and were dropped from hippocampus analyses after the previously described adjustments did not fix the issue (2 young, 1 older). Moreover, four participants exhibited globus pallidus segmentation issues in diffusion space which could not be corrected, and they were dropped from globus pallidus analyses (3 young, 1 older). One participant exhibited a misalignment (>1 voxel displacement) for the caudate in magnitude space, and they were dropped from caudate analyses. No individual participant was excluded from more than 2 region analyses.

2.6. Diffusion data pre-processing

For each participant, diffusion data were pre-processed using the FMRIB Software Library (FSL) and the Analysis of Functional Neuro Images (AFNI) suite [34–36]. AFNI's 3D skull strip was used to remove non-brain tissue and generate a whole brain mask in the b = 0 image. Standard preprocessing steps were applied to correct for motion, eddy-current induced distortions, and susceptibility induced distortions in the DTI data using eddy in FSL [30,37]. b = 0 images from the two diffusion acquisitions were input into FSL's topup and a field map was generated for susceptibility distortion correction. Uncorrected DTI data were input into FSL's EDDY and data were corrected for eddy currents, susceptibility artifacts, and gross motion correction.

Pre-processed data were then analyzed using the NODDI MATLAB toolbox (http://mig.cs.ucl.ac.uk/index.php) to acquire diffusion compartment estimates. A two-stage approach was used to separate the diffusion signal into three compartments: restricted (also known as intracellular volume fraction [fICVF] or neurite density index [NDI]), hindered (also known as orientation dispersion index, ODI), and free (also known as fraction of isotropic diffusion, fISO) diffusion [12,38]. During the first stage, the total diffusion signal was separated into tissue and non-tissue diffusion compartments, with the non-tissue component modeled as an isotropic sphere (free diffusion). During the second stage, the tissue component was further separated into restricted and hindered diffusion components, which are characterized as sticks and the dispersion of sticks respectively. Outputs included voxel-wise images of free, hindered, and restricted diffusion for each participant.

2.7. R_2* (Iron) data pre-processing

GRE images were analyzed with a custom MATLAB script. R_2* for each voxel was calculated by fitting the signal decay from the 12-echo GRE data to a monoexponential model, $S_i = S_0 \exp(-R_2^* TE)$. Note that S_i indicates the signal of a voxel at the ith echo time and S_0 indicates a fitting constant.

2.8. Acquiring diffusion metrics and R_2* values from ROIs

Free, hindered, and restricted diffusion metrics as well as R_2* values were extracted separately from bilateral regions of interest (ROI; caudate, putamen, nucleus accumbens, globus pallidus, and hippocampus) for each participant. Free diffusion metrics were acquired by multiplying each bilateral diffusion space-aligned ROI mask by the voxel-wise free diffusion image before taking the average across voxels.

An inclusion mask was created for the remaining diffusion metrics by thresholding the free diffusion image to exclude voxels with low tissue content (free diffusion > 90 %). Hindered and restricted diffusion metrics were then acquired by multiplying each bilateral diffusion space-aligned ROI mask by these inclusion masks and then by the corresponding voxel-wise diffusion images before taking the average across voxels. Bilateral diffusion metrics were then averaged to generate one diffusion metric per region per participant.

R_2* values were extracted separately from bilateral ROIs for each participant using the same approach. Each bilateral aligned ROI mask was multiplied by the voxel-wise R_2* map before taking the average across voxels and mean R_2* was obtained for each participant.

3. Results

3.1. Behavioral results

3.1.1. Age group differences in early versus late learning

To assess age group differences in IAL as a function of learning stage, Learning Stage (Early, Late) x Triplet Type (HF, LF) x Age Group (Young, Old) repeated measures ANOVAs were conducted separately for mean accuracy and log-transformed mean of median RTs (see Fig. 2). Learning Stage and Triplet Type varied within-subjects while Age Group varied between-subjects.

For mean accuracy, a significant main effect of Age Group (F (1, 59) = 5.10, p = 0.03, η_p^2 = 0.08), indicated that young adults (89.60 % ± 1.60) were more accurate than older adults (84.10 % ± 1.80). A significant Learning Stage x Age Group interaction (F (1, 59) = 6.26, p = 0.02, η_p^2 = 0.10) showed that the difference in accuracy for early versus late learning was smaller in young adults (Early: 90.30 % ± 1.90, Late: 89.00 % ± 1.60; Mean Difference = -1.30 %) compared to older adults (Early: 82.10 % ± 2.20, Late: 86.20 % ± 1.90; Mean Difference = 4.10 %). No other effects attained significance (ps > 0.21).

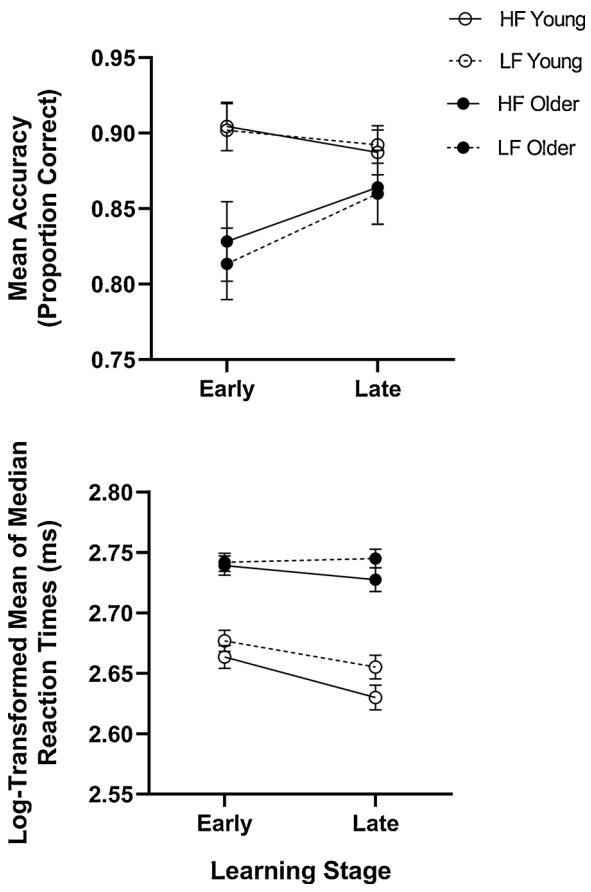

Fig. 2. Associative learning performance. Mean accuracy (top) and mean of median log-transformed reaction times (bottom) to high frequency (HF, solid line) and low-frequency (LF, dashed line) triplets are shown separately for young (open circle) and older (closed circle) adults. Error bars denote standard error of the means. Significant learning was seen as faster (but not more accurate) responses to HF versus LF triplets, particularly in the late learning stage, with a significantly larger learning effect for young versus older adults.

For reaction time, there was also a significant main effect of Age Group (F (1, 59) = 44.16, p < 0.001, η_p^2 = 0.43), indicating that younger adults (2.66 ± 0.01) were faster than older adults (2.74 ± 0.01) overall, as is typical. Significant effects of Learning Stage (F (1, 59) = 16.13, p < 0.001, η_p^2 = 0.22) and Learning Stage x Age Group (F (1, 59) = 8.82, p = 0.004, η_p^2 = 0.13) were consistent with age group differences in skill learning. That is, RTs were faster in late learning (2.69 ± 0.01) compared to early learning (2.71 ± 0.01) and this difference was larger in young (Early: 2.67 ± 0.01, Late: 2.64 ± 0.01; Mean Difference = 0.03) compared to older (Early: 2.74 ± 0.01, Late: 2.74 ± 0.01; Mean Difference = 0.004) adults. Significant effects of Triplet Type (F (1, 59) = 57.32, p < 0.001, η_p^2 = 0.50), Triplet Type x Learning Stage (F (1, 59) = 18.60, p < 0.001, η_p^2 = 0.24), and Triplet Type x Age Group (F (1, 59) = 5.57, p = 0.022, η_p^2 = 0.09) were consistent with age group differences in learning the associations. RTs were faster to HF triplets (2.69 ± 0.01) compared to LF triplets (2.71 ± 0.01). This learning effect was larger in late learning (HF: 2.68 ± 0.01; LF: 2.70 ± 0.01; Mean Difference = 0.02) relative to early learning (2.70 ± 0.01 versus 2.71 ± 0.01; Mean Difference = 0.01) and in young adults (HF: 2.65 ± 0.01; LF: 2.67 ± 0.01; Mean Difference = 0.02) relative to older adults (2.73 ± 0.01 versus 2.74 ± 0.01; Mean Difference = 0.01). However, the Learning Stage x Triplet Type x Age Group interaction did not reach significance (p = 0.634).

3.1.2. No explicit awareness

To test for explicit knowledge that HF triplets occur more frequently than LF triplets, a Triplet Type (HF, LF, NF) x Age Group (Young, Old) repeated measures ANOVA was conducted on mean response scores (calculated as the average of 'frequently', 'infrequently', and 'not at all' recognition judgements recoded as 2, 1, and 0, respectively).

A significant effect of Triplet Type (F (2, 114) = 94.18, p < 0.001, η_p^2 = 0.623), probed using pairwise comparisons, revealed no difference in mean response scores for HF compared to LF triplets (HF: 1.57 ± 0.05, LF: 1.53 ± 0.05; Mean Difference = 0.037; p = 0.405), but significant differences between mean response scores for NF triplets (NF: 0.832 ± 0.07) compared to HF (Mean Difference = 0.73; p < 0.001) and LF triplets (Mean Difference = 0.70; p < 0.001), indicating no difference in recognition judgements for HF and LF triplets even as participants endorse NF triplets as not having occurred frequently or at all. A significant Triplet Type x Age Group interaction (F (2, 114) = 5.81, p = 0.004, η_p^2 = 0.09) further revealed that older adults had significantly lower LF (1.42 ± 0.07) mean response scores compared to young adults (1.64 ± 0.06; Mean Difference = 0.23; p = 0.031), but showed no difference in HF or NF triplet mean response scores (ps > 0.213), indicating a potential bias among older adults toward rating LF triplets as occurring more infrequently compared to young adults. No other effects approached significance (ps > 0.450).

Additional evidence that participants had no explicit awareness of the associations was found in their interview responses, in that no participant was able to accurately describe any relationship between the cues and targets.

3.2. Age group differences in gray matter microstructure

We used one-way ANCOVAs to assess whether gray matter microstructure varied by age group, with age group as a fixed factor, separately for each diffusion metric (free, hindered, restricted) in each ROI (caudate, putamen, nucleus accumbens, globus pallidus, hippocampus) while controlling for iron content in that region (see Fig. 3).

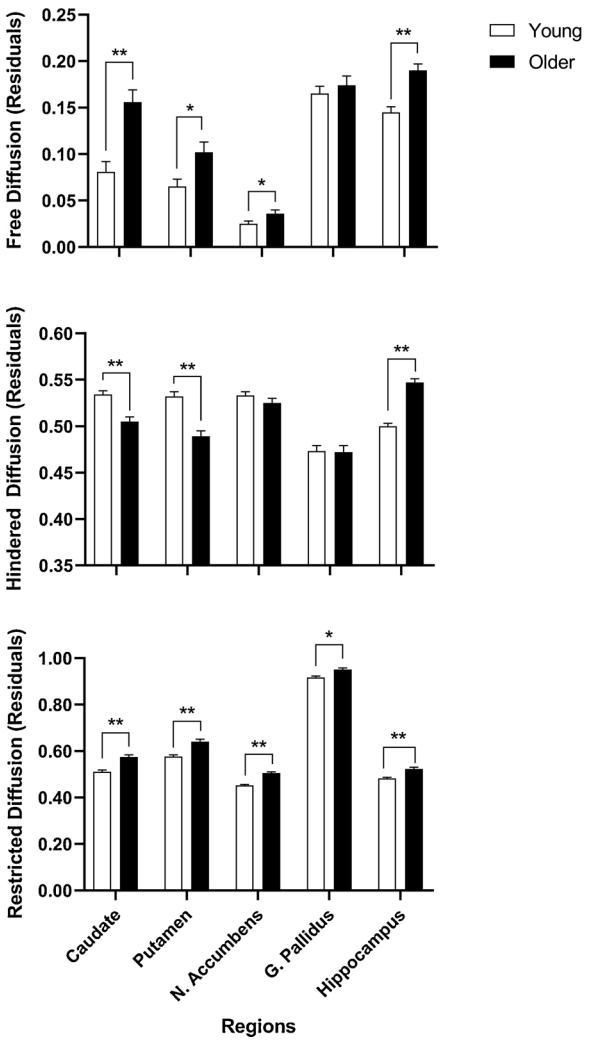

Fig. 3. Age-related differences in diffusion. Diffusion metrics (free, hindered, restricted; controlled for region specific iron content) for basal ganglia and hippocampus regions of interest in young (white bar) and older (black bar) adults are shown separately. Error bars denote standard error of the means. The caudate, putamen, and hippocampus showed significant age group differences across all metrics, although the direction of these effects differed for hindered diffusion. ** = $p < 0.001$, * = $p < 0.05$.

The caudate revealed significantly higher free (F (1, 52) = 15.54, $p < 0.001$, $\eta_p^2 = 0.23$) and restricted (F (1, 52) = 21.66, $p < 0.001$, $\eta_p^2 = 0.29$) diffusion and significantly lower hindered diffusion (F (1, 52) = 14.94, $p < 0.001$, $\eta_p^2 = 0.22$) in older versus young adults. The putamen also exhibited significantly higher free (F (1, 56) = 5.20, $p = 0.026$, $\eta_p^2 = 0.09$) and restricted (F (1, 56) = 15.67, $p < 0.001$, $\eta_p^2 = 0.22$) diffusion and significantly lower hindered diffusion (F (1, 56) = 23.07, $p < 0.001$, $\eta_p^2 = 0.29$) in older versus young adults. Similarly, the hippocampus revealed significantly higher free (F (1, 53) = 24.75, $p < 0.001$, $\eta_p^2 = 0.32$), hindered (F (1, 53) = 100.52, $p < 0.001$, $\eta_p^2 = 0.66$), and restricted (F (1, 53) = 21.76, $p < 0.001$, $\eta_p^2 = 0.29$) diffusion in older versus young adults. For the nucleus accumbens, results revealed significantly higher free (F (1, 56) = 4.85, $p = 0.032$, $\eta_p^2 = 0.08$) and restricted (F (1, 56) = 73.03, $p < 0.001$, $\eta_p^2 = 0.57$) diffusion in older versus young adults, but no group difference for hindered diffusion ($p = 0.271$). For the globus pallidus, results revealed significantly higher restricted diffusion (F (1, 53) = 12.23, $p = 0.001$, $\eta_p^2 = 0.19$) in older versus young adults, but no group difference for free ($p = 0.509$) or hindered ($p = 0.906$) diffusion. These results demonstrate effects of aging on at least one diffusion metric for all regions of interest, with age-related decreases in hindered diffusion for the caudate and putamen potentially signaling a unique neural substrate (e.g., moderate accumulation of iron throughout the lifespan).

3.3. Age-independent relationships between IAL scores and gray matter microstructure

We first assessed relationships between IAL and gray matter microstructure separately in each age group. Partial correlations were conducted between each IAL score (early, late) and each diffusion metric (free, hindered, restricted) from each ROI (caudate, putamen, nucleus accumbens, globus pallidus, hippocampus) while controlling for iron content in that region separately for young and older adults (see Fig. 4 and Table 2). Significant effects were Bonferroni corrected for three comparisons per dependent measure for each ROI ($p < 0.017$). Results include both significant and trending ($p < 0.05$) effects.

For young adults, early IAL scores were significantly positively related to restricted caudate diffusion (r = 0.471, $p = 0.009$). Results also showed that late IAL scores marginally related to hindered caudate diffusion (r = 0.407, $p = 0.026$) and restricted globus pallidus diffusion (r = 0.420, $p = 0.019$). No other correlations attained significance ($ps > 0.064$).

For older adults, late IAL scores were significantly related to hindered globus pallidus diffusion (r = 0.516, $p = 0.014$). Results also showed that late IAL scores marginally were related to hindered hippocampus diffusion (r = 0.466, $p = 0.033$). No other correlations approached significance ($ps > 0.338$). Thus, better early and late learning was associated with higher basal ganglia diffusion in both age groups (caudate and/or globus pallidum), with better late learning also relating to higher hippocampal diffusion in older adults.

3.4. Age-dependent relationships between IAL scores and gray matter microstructure

We then examined whether age group moderated relationships between IAL scores and gray matter microstructure for any significant or trending effects reported in the previous section (see Figure 4) via separate multiple regression models which included age group, the diffusion metric, and the age group x diffusion metric interaction as predictor variables; iron content as a covariate; and the IAL score as the dependent variable.

The interaction terms for the relationship between early IAL and restricted caudate diffusion ($\Delta R^2 = .06$, ΔF (1, 50) = 3.90, b = -1.08, t (50) = -1.98, $p = 0.054$) and between late IAL and hindered hippocampus diffusion ($\Delta R^2 = .07$, ΔF (1, 50) = 3.99, $b = 1.63$, t (50) = 1.99, $p = 0.051$) were only marginally significant, indicating that age did not significantly moderate any of the learning-diffusion relationships. No other interactions approached significance ($ps > 0.338$). Moreover, reanalyzing these data using a Bayesian test provided additional, strong evidence in favor of there being no difference in previously reported learning-diffusion relationships between young and older adults (see Supplementary Tables 1 and 2).

4. Discussion

The present study examined age group differences in IAL as a function of learning stage, age group differences in basal ganglia and hippocampal gray matter microstructure, relationships between IAL and gray matter microstructure across age groups, and whether these IAL-microstructure relationships were moderated by age. We extended earlier work by assessing microstructure of subcortical gray matter and by controlling for iron content, which is known to increase with age [24, 39–42], affect diffusion [23,25], and relate to learning [11]. In line with our predictions, older adults exhibited deficits in IAL and differences in diffusion across all three metrics for the basal ganglia (caudate, putamen) and hippocampus compared to young adults. Further, diffusion in

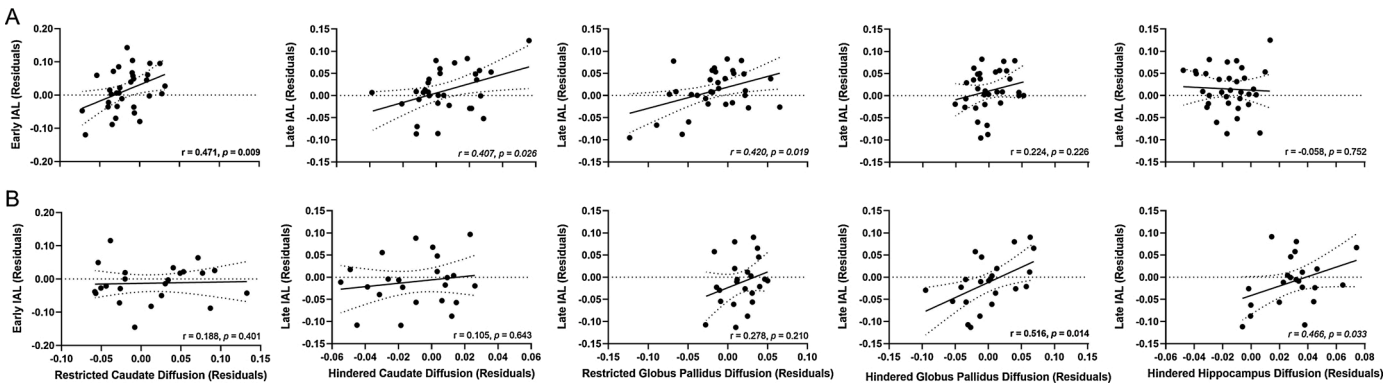

Fig. 4. Relationships between learning and diffusion. Significant (bolded) and trending (italicized) correlations between early (left) and late (middle, right) log-transformed IAL scores and diffusion metrics (controlled for region specific iron content) are shown separately for young (A, top) and older (B, bottom) adults. Dotted lines denote 95 % confidence interval bands. Importantly, none of these relationships were significantly moderated by age group.

Table 2
Correlation coefficients between IAL scores and diffusion metrics.

	Young		Older	
Diffusion Metric/ROI	Early IAL	Late IAL	Early IAL	Late IAL
Free Diffusion				
Caudate	0.34	−0.01	−0.01	0.13
Putamen	0.14	0.13	−0.24	0.14
Nucleus Accumbens	0.30	0.02	0.09	0.26
Globus Pallidus	0.06	0.07	−0.24	−0.04
Hippocampus	0.19	−0.05	−0.18	0.18
Hindered Diffusion				
Caudate	0.33	*0.41*	−0.24	0.11
Putamen	0.32	−0.01	−0.01	−0.24
Nucleus Accumbens	0.09	0.19	0.06	−0.11
Globus Pallidus	0.08	0.22	0.37	**0.52**
Hippocampus	0.04	−0.06	0.22	*0.47*
Restricted Diffusion				
Caudate	**0.47**	0.19	0.19	0.21
Putamen	0.12	0.19	−0.22	0.27
Nucleus Accumbens	0.30	0.22	0.03	−0.16
Globus Pallidus	0.33	*0.42*	0.10	0.28
Hippocampus	0.30	0.07	−0.17	0.12

Note. Significant ($p < 0.017$, Bonferroni-corrected; bolded) and trending ($p < 0.05$; italicized) correlation coefficients between log-transformed reaction time implicit associative learning (IAL) scores and diffusion metrics (free, hindered, restricted) from each region of interest (ROI) are shown separately for each age group (young, older) and learning stage (early, late), after controlling for region-specific iron content.

the basal ganglia, but not hippocampus, was significantly related to early IAL in young adults (caudate) and late IAL in older adults (globus pallidum). However, none of the IAL-diffusion relationships were significantly moderated by age, indicating that basal ganglia microstructure contributes to IAL performance across the lifespan.

IAL was seen across age groups as faster responses to more versus less frequently occurring triplets (HF versus LF) that increased from the early to late learning stage, with this Trial Type difference being smaller for older versus younger adults. Although these learning and age effects are comparable to those seen in previous studies, we did not observe the expected three-way interaction between Age Group, Trial Type, and Learning Stage [7,6,9]. This may be due to the comparatively shorter number of trials utilized in this version of the TLT, as one study has indicated extensive practice is associated with age differences in IAL [43]. However, at least one other dataset that also shortened the TLT for MRI did observe a significant three-way interaction [27,28,9], indicating that our finding was not influenced solely by the reduced number of trials. Instead, our pattern of results is likely due to differences in triplet complexity. Truly probabilistic sequences that include all possible combinations of cue-target associations have used 64 unique triplets that occur with a range of different frequencies [6]. In contrast, the current TLT version used just 12 unique triplets (4 HF, 8 LF), which is also fewer than the 18 used in the previous TLT MRI study [9]. Moreover, our counterbalanced, pseudo-random structure ensured that there was no overlap between cues that predicted target locations for HF and LF triplets, eliminating triplet combinations that occurred with other frequencies. Previous studies using similar, more deterministic sequences (utilizing the Serial Reaction Time Task, SRTT) have also shown no age-related differences in IAL [44,45]. Whereas learning effects are consistently seen for reaction time, our lack of learning for accuracy was not unexpected given previous reports of both significant [6,27] and non-significant [5,9] learning effects, which may also result from differences in triplet complexity among other factors (e.g. whether feedback is used to maintain accuracy, predictive order structure). Importantly, our ability to replicate earlier work demonstrates that shortened, less complex (i.e., fewer unique triplets, deterministic regularity) TLT versions, as used here, are appropriate for detecting significant learning and age group differences in learning within the constraints of the MRI environment.

We further observed age group differences in hippocampal and basal ganglia gray matter microstructure. For the hippocampus, our finding of higher free, hindered, and restricted diffusion in older relative to young adults reflects previous reports of age-related increases in one [15,17,18] or all [19] NODDI metrics. For the basal ganglia, most regions exhibited higher free and restricted diffusion in older relative to young adults with either an age-related decrease (caudate, putamen) or no age group difference (nucleus accumbens) in hindered diffusion, whereas one region showed only an age-related increase in restricted diffusion (globus pallidus). At least two previous studies similarly found that older adults have lower hindered diffusion in the striatum (particularly caudate) than young adults [15,20], although we are the first to examine age effects on microstructure across multiple basal ganglia regions. Previous studies of gray matter microstructure have interpreted variations in diffusion as reflecting differences in neurite complexity [21,22], myelin density [46], or dendritic processes [47], all of which are affected by aging. However, in the absence of comprehensive diffusion-histology research that can more accurately link biological substrates to the individual diffusion metrics, we can only posit that numerous neurobiological factors (e.g. neurite density, glial cells, cell swelling/shrinkage, and vascular changes) contribute to the observed age-related diffusion effects [21,22].

One neurobiological factor of particular interest here is iron, given that it accumulates in basal ganglia regions with age [23,25,40–42], attenuates the diffusion signal at acquisition [25], and relates to various cognitive functions [24,41,48], including IAL [11]. Interestingly, hindered diffusion, which showed the most variability in age effects across regions, appeared to track with the presence of iron. That is, the region

that accumulates minimal amounts of iron showed an age-related increase in hindered diffusion (hippocampus), regions that gradually accumulate a moderate amount of iron throughout the lifespan showed an age-related decrease in hindered diffusion (caudate, putamen), and the region that accumulates the most iron by early adulthood and plateaus across the lifespan showed no effect of age on hindered diffusion (globus pallidus) [49]. Of note, we attempted to minimize the potential confounding effect of iron by statistically controlling for its concentration in our diffusion metrics. However, it remains possible that iron attenuates the diffusion signal at the time of acquisition [25], which may be driving these results for hindered diffusion. As such, it will be necessary to develop a diffusion sequence that is insensitive to iron in order to fully understand the effect of age on diffusion in regions with high iron concentration.

After statistically controlling for these iron effects, we provide support for basal ganglia involvement in IAL using NODDI measures of gray matter microstructure. Specifically, we observed that early IAL was significantly correlated with restricted caudate diffusion in young adults, whereas late IAL was significantly correlated with hindered globus pallidus diffusion in older adults. Marginally significant relationships were also observed between late IAL and hindered caudate and restricted globus pallidus diffusion in young adults, and hindered hippocampus diffusion in older adults. Larger learning effects in late compared to early IAL may have contributed to its apparent sensitivity to diffusion. Notably, none of these relationships were significantly moderated by age, indicating similar gray matter microstructural substrates of IAL in young and older adults. These results coincide with a growing body of functional [9,11,44,50–53], structural [10], and genotypic [28] evidence showing that basal ganglia (particularly caudate) relates to both early and late stages of learning. Moreover, our finding that globus pallidus, not just caudate, microstructure contributes to IAL performance is consistent with emerging work [11,53], potentially signifying that later learning is affected by differences in the presence of iron or other microstructural alterations like dendritic arborization that may have a larger impact on extracellular sources of diffusion captured by the hindered diffusion metric. In contrast, early learning may be impacted by differences in neurite density or other intracellular neurobiological substrates captured by the restricted diffusion metric in caudate. The directionality of these findings likely results from direct connections between these regions [54,55], with caudate involved in the early acquisition of the cue-target associations and globus pallidus engaged later in learning.

Although we did observe a trending relationship between hindered hippocampus diffusion and late IAL, we were not able to replicate previous findings implicating hippocampal involvement in early learning [9,51]. This may be due to the relatively small learning effect in early IAL, although we were able to detect a significant relationship between early IAL and restricted caudate diffusion in young adults. Alternatively, static measures of hippocampal gray matter diffusion may be less sensitive than dynamic measures of its activity during IAL, although we were previously able to detect a significant relationship between IAL and integrity of white matter tracts emanating from the hippocampus [10]. The contribution of hippocampal structure and function to early and late IAL will benefit from future multimodal imaging research.

The positive nature of the significant IAL-basal ganglia diffusion relationships was unexpected. Previous NODDI studies of white matter integrity typically find negative relations to cognition, with lower diffusion (thought to reflect better integrity) relating to better performance [18]. Comparable studies of hippocampal gray matter also report negative relationships between diffusion and performance [18,56]. That said, at least one study observed a positive correlation between hippocampus hindered diffusion and a measure of processing speed and working memory performance [15], and another study of basal ganglia gray matter observed both negative and positive diffusion-performance relationships, with lower and higher restricted putamen diffusion relating to goal-directed and habitual decision-making, respectively [57]. Because these positive relationships have been observed in subcortical gray matter structures with (basal ganglia) and without (hippocampus) significant iron concentrations, and the same region can show positive and negative relationships to cognition (putamen), it is unlikely that this result reflects regional differences in microstructural properties. Instead, we suspect that the nature of the cognitive measure and the corresponding behavioral measures drive the direction of diffusion-performance relationships.

5. Conclusion

In this first examination of relationships between IAL and gray matter microstructure in the basal ganglia and hippocampus, we found that older adults had worse IAL and disrupted diffusion in all subcortical regions relative to young adults. More importantly, early and late stage IAL was significantly related to caudate and globus pallidus microstructure, respectively, with minimal evidence that these IAL-microstructure relationships vary with age. Even though age has a significant effect on both IAL performance and the microstructure of subcortical regions, it is individual differences in diffusion that affect implicit learning, independent of age groups.

Data statement

The data that support the findings of this study are available from the corresponding author upon reasonable request.

Funding

This work was supported by R00 AG047334 (Bennett) and R21 AG054804 (Bennett) from the National Institutes of Health/National Institute on Aging.

CRediT authorship contribution statement

Corinna Y. Franco: Conceptualization, Methodology, Formal analysis, Investigation, Data curation, Writing - original draft, Visualization. **Jessica R. Petok:** Formal analysis, Writing - review & editing. **Jason Langley:** Formal analysis, Writing - review & editing. **Xiaoping Hu:** Writing - review & editing. **Ilana J. Bennett:** Conceptualization, Methodology, Formal analysis, Investigation, Resources, Writing - review & editing, Supervision, Project administration, Funding acquisition.

Declaration of Competing Interest

None.

Acknowledgements

The authors wish to thank Cheslea Evelyn for help with data acquisition and Justino Flores for his role in data collection.

References

[1] Carol A. Seger, Implicit learning, Psychol. Bull. 115 (1994) 163–196, https://doi.org/10.1037/0033-2909.115.2.163.
[2] K. Foerde, D. Shohamy, The role of the basal ganglia in learning and memory: insight from Parkinson's disease, Neurobiol. Learn. Mem. 96 (2011) 624–636, https://doi.org/10.1016/j.nlm.2011.08.006.
[3] P.K. Kuhl, Early language acquisition: cracking the speech code, Nat. Rev. Neurosci. 5 (2004) 831–843, https://doi.org/10.1038/nrn1533.
[4] M.D. Lieberman, Intuition : a social cognitive neuroscience approach logic of intuition as implicit learning, Psychol. Bull. 126 (2000) 109–137, https://doi.org/10.1037//0033-2909.126.1.109.
[5] C.M. Stillman, J.H. Howard, D.V. Howard, The effects of structural complexity on age-related deficits in implicit probabilistic sequence learning, J. Gerontol. - Series B Psychol. Sci. Soc. Sci. 71 (2016) 212–219, https://doi.org/10.1093/geronb/gbu135.

[6] J.H. Howard, D.V. Howard, N.A. Dennis, A.J. Kelly, Implicit learning of predictive relationships in three-element visual sequences by young and old Adults, J. Exp. Psychol. Learn. Mem. Cogn. 34 (2008) 1139–1157, https://doi.org/10.1037/a0012797.

[7] A.B. Forman-Alberti, K.L. Seaman, D.V. Howard, J.H. Howard, Event simultaneity does not eliminate age deficits in implicit probabilistic sequence learning, Int. J. Aging Hum. Dev. 79 (2014) 211–223, https://doi.org/10.2190/AG.79.3.b.

[8] K. Janacsek, J. Fiser, D. Nemeth, The best time to acquire new skills: age-related differences in implicit sequence learning acr oss the human lifespan, Dev. Sci. 15 (2012) 496–505, https://doi.org/10.1111/j.1467-7687.2012.01150.x.

[9] J.R. Simon, C.J. Vaidya, J.H. Howard, D.V. Howard, The effects of aging on the neural basis of implicit associative learning in a probabilistic triplets learning task, J. Cogn. Neurosci. 24 (2012) 451–463, https://doi.org/10.1162/jocn_a_00116.

[10] I.J. Bennett, D.J. Madden, C.J. Vaidya, J.H. Howard, D.V. Howard, White matter integrity correlates of implicit sequence learning in healthy aging, Neurobiol. Aging 32 (2011) 2317, https://doi.org/10.1016/j.neurobiolaging.2010.03.017, e1-2317.e12.

[11] J. Persson, B. Garzón, R. Sitnikov, L. Bäckman, G. Kalpouzos, A positive influence of basal ganglia iron concentration on implicit sequence learning, Brain Struct. Funct. 225 (2020) 735–749, https://doi.org/10.1007/s00429-020-02032-7.

[12] H. Zhang, T. Schneider, C.A. Wheeler-Kingshott, D.C. Alexander, NODDI: practical in vivo neurite orientation dispersion and density imaging of the human brain, NeuroImage 61 (2012) 1000–1016, https://doi.org/10.1016/j.neuroimage.2012.03.072.

[13] H. Fukutomi, M.F. Glasser, H. Zhang, J.A. Autio, T.S. Coalson, T. Okada, T. Hayashi, Neurite imaging reveals microstructural variations in human cerebral cortical gray matter, NeuroImage 182 (2018) 488–499, https://doi.org/10.1016/j.neuroimage.2018.02.017.

[14] A.P. Merluzzi, D.C. Dean, N. Adluru, G.S. Suryawanshi, O.C. Okonkwo, J.M. Oh, B. B. Bendlin, Age-dependent differences in brain tissue microstructure assessed with neurite orientation dispersion and density imaging, Neurobiol. Aging 43 (2016) 79–88, https://doi.org/10.1016/j.neurobiolaging.2016.03.026.

[15] X. Nazeri, M. Chakravart, D.J. Rotenberg, T.K. Rajji, X. Rathi, O.V. Michailovich, A. N. Voineskos, Functional consequences of neurite orientation dispersion and density in humans across the adult lifespan, J. Neurosci. 35 (2015) 1753–1762, https://doi.org/10.1523/JNEUROSCI.3979-14.2015.

[16] Y. Rathi, O. Pasternak, P. Savadjiev, O. Michailovich, S. Bouix, M. Kubicki, M. E. Shenton, Gray matter alterations in early aging: a diffusion magnetic resonance imaging study, Hum. Brain Mapp. 35 (2014) 3841–3856, https://doi.org/10.1002/hbm.22441.

[17] C. Metzler-Baddeley, J.P. Mole, R. Sims, F. Fasano, J. Evans, D.K. Jones, R. J. Baddeley, Fornix white matter glia damage causes hippocampal gray matter damage during age-dependent limbic decline, Sci. Rep. 9 (2019) 1–14, https://doi.org/10.1038/s41598-018-37658-5.

[18] H. Radhakrishnan, S.M. Stark, C.E.L. Stark, Microstructural alterations in hippocampal subfields mediate age-related memory decline in humans, Front. Aging Neurosci. 12 (2020) 94, https://doi.org/10.3389/fnagi.2020.00094.

[19] A. Venkatesh, S.M. Stark, C.E.L. Stark, I.J. Bennett, Hippocampal gray matter integrity declines in healthy aging and relates to mnemonic discrimination, Neurobiol. Aging (2020).

[20] M. Ota, N. Sato, N. Maikusa, D. Sone, H. Matsuda, H. Kunugi, Whole brain analyses of age-related microstructural changes quantified using different diffusional magnetic resonance imaging methods, J. Radiol. 35 (2017) 584–589, https://doi.org/10.1007/s11604-017-0670-7.

[21] F. Grussu, T. Schneider, C. Tur, R.L. Yates, M. Tachrount, A. Ianuş, C.A.M. Gandini Wheeler-Kingshott, Neurite dispersion: a new marker of multiple sclerosis spinal cord pathology? Ann. Clin. Transl. Neurol. 4 (2017) 663–679, https://doi.org/10.1002/acn3.445.

[22] K. Sato, A. Kerever, K. Kamagata, K. Tsuruta, R. Irie, K. Tagawa, S. Aoki, Understanding microstructure of the brain by comparison of neurite orientation dispersion and density imaging (NODDI) with transparent mouse brain, Acta Radiol. Open 6 (2017), https://doi.org/10.1177/2058460117703816, 2058460117703816.

[23] J. Langley, S. Hussain, J.J. Flores, I.J. Bennett, X. Hu, Characterization of age-related microstructural changes in locus coeruleus and substantia nigra pars compacta, Neurobiol. Aging 87 (2020) 89–97, https://doi.org/10.1016/j.neurobiolaging.2019.11.016.

[24] A.M. Daugherty, E.M. Haacke, N. Raz, Striatal iron content predicts its shrinkage and changes in verbal working memory after two years in healthy adults, J. Neurosci. 35 (2015) 6731–6743, https://doi.org/10.1523/JNEUROSCI.4717-14.2015.

[25] E.M. Haacke, N.Y.C. Cheng, M.J. House, Q. Liu, J. Neelavalli, R.J. Ogg, A. Obenaus, Imaging iron stores in the brain using magnetic resonance imaging, Magn. Reson. Imaging 23 (2005) 1–25, https://doi.org/10.1016/j.mri.2004.10.001.

[26] S.T. Pendlebury, S.J.V. Welch, F.C. Cuthbertson, J. Mariz, Z. Mehta, P.M. Rothwell, Telephone assessment of cognition after transient ischemic attack and stroke: Modified telephone interview of cognitive status and telephone montreal cognitive assessment versus face-to-face montreal cognitive assessment and neuropsychological battery, Stroke 44 (2013) 227–229, https://doi.org/10.1161/STROKEAHA.112.673384.

[27] J.R. Simon, J.H. Howard, D.V. Howard, Age differences in implicit learning of probabilistic unstructured sequences, J. Gerontol. - Series B Psychol. Sci. Soc. Sci. 66 (B) (2011) 32–38, https://doi.org/10.1093/geronb/gbq066.

[28] J.R. Simon, M. Stollstorff, L.C. Westbay, C.J. Vaidya, J.H. Howard, D.V. Howard, Dopamine transporter genotype predicts implicit sequence learning, Behav. Brain Res. 216 (2011) 452–457, https://doi.org/10.1016/j.bbr.2010.08.043.

[29] M.A. Griswold, P.M. Jakob, R.M. Heidemann, M. Nittka, V. Jellus, J. Wang, A. Haase, Generalized autocalibrating partially parallel acquisitions (GRAPPA), Magn. Reson. Med. 47 (2002) 1202–1210, https://doi.org/10.1002/mrm.10171.

[30] J.L.R. Andersson, S. Skare, J. Ashburner, How to correct susceptibility distortions in spin-echo echo-planar images: application to diffusion tensor imaging, NeuroImage 20 (2003) 870–888, https://doi.org/10.1016/S1053-8119(03)00336-7.

[31] B. Patenaude, S.M. Smith, D.N. Kennedy, M. Jenkinson, A Bayesian model of shape and appearance for subcortical brain segmentation, NeuroImage 56 (2011) 907–922, https://doi.org/10.1016/j.neuroimage.2011.02.046.

[32] B. Patenaude, Bayesian Statistical Models of Shape and Appearance for Subcortical Brain Segmentation, 2007.

[33] X. Feng, A. Deistung, M.G. Dwyer, J. Hagemeier, P. Polak, J. Lebenberg, F. Schweser, An improved FSL-FIRST pipeline for subcortical gray matter segmentation to study abnormal brain anatomy using quantitative susceptibility mapping (QSM), Magn. Reson. Imaging 39 (2017) 110–122, https://doi.org/10.1016/j.mri.2017.02.002.

[34] R.W. Cox, J.S. Hyde, Software tools for analysis and visualization of fMRI data, NMR Biomed. 10 (1997) 171–178, https://doi.org/10.1002/(SICI)1099-1492(199706/08)10:4/5<171::AID-NBM453>3.0.CO;2-L.

[35] M. Jenkinson, C.F. Beckmann, T.E.J. Behrens, M.W. Woolrich, S.M. Smith, Review FSL, NeuroImage 62 (2012) 782–790, https://doi.org/10.1016/j.neuroimage.2011.09.015.

[36] S.M. Smith, M. Jenkinson, M.W. Woolrich, C.F. Beckmann, T.E.J. Behrens, H. Johansen-Berg, P.M. Matthews, Advances in functional and structural MR image analysis and implementation as FSL, NeuroImage 23 (2004) S208–S219, https://doi.org/10.1016/j.neuroimage.2004.07.051.

[37] J.L.R. Andersson, S.N. Sotiropoulos, An integrated approach to correction for off-resonance effects and subject movement in diffusion MR imaging, NeuroImage 125 (2016) 1063–1078, https://doi.org/10.1016/j.neuroimage.2015.10.019.

[38] M. Tariq, T. Schneider, D.C. Alexander, C.A. Gandini Wheeler-Kingshott, H. Zhang, Bingham-NODDI: mapping anisotropic orientation dispersion of neurites using diffusion MRI, NeuroImage 133 (2016) 207–223, https://doi.org/10.1016/j.neuroimage.2016.01.046.

[39] E.M. Haacke, Y. Miao, M. Liu, C.A. Habib, Y. Katkuri, T. Liu, J. Wu, Correlation of putative iron content as represented by changes in R2* and phase with age in deep gray matter of healthy adults, J. Magn. Reson. Imaging 32 (2010) 561–576, https://doi.org/10.1002/jmri.22293.

[40] A. Pfefferbaum, E. Adalsteinsson, T. Rohlfing, E.V. Sullivan, Diffusion tensor imaging of deep gray matter brain structures: effects of age and iron concentration, Neurobiol. Aging 31 (2010) 482–493, https://doi.org/10.1016/j.neurobiolaging.2008.04.013.

[41] K.M. Rodrigue, A.M. Daugherty, E.M. Haacke, N. Raz, The role of hippocampal iron concentration and hippocampal volume in age-related differences in memory, Cereb. Cortex 23 (2012) 1533–1541, https://doi.org/10.1093/cercor/bhs139.

[42] L. Zecca, M.B.H. Youdim, P. Riederer, J.R. Connor, R.R. Crichton, Iron, brain ageing and neurodegenerative disorders, Nat. Rev. Neurosci. 5 (2004) 863–873, https://doi.org/10.1038/nrn1537.

[43] D.V. Howard, J.H. Howard, K. Japikse, C. DiYanni, A. Thompson, R. Somberg, Implicit sequence learning: effects of level of structure, adult age, and extended practice, Psychol. Aging 19 (2004) 79–92, https://doi.org/10.1037/0882-7974.19.1.79.

[44] N.A. Dennis, R. Cabeza, Age-related dedifferentiation of learning systems: an fMRI study of implicit and explicit learning, Neurobiol. Aging 32 (2011) 2318, https://doi.org/10.1016/j.neurobiolaging.2010.04.004, e17-2318.e30.

[45] V. Gaillard, A. Destrebecqz, S. Michiels, A. Cleeremans, Effects of age and practice in sequence learning: a graded account of ageing, learning, and control, Eur. J. Cogn. Psychol. 21 (2009) 255–282, https://doi.org/10.1080/09541440802257423.

[46] N. Wang, J. Zhang, G. Cofer, Y. Qi, R.J. Anderson, L.E. White, G. Allan Johnson, Neurite orientation dispersion and density imaging of mouse brain microstructure, Brain Struct. Funct. 224 (2019) 1797–1813, https://doi.org/10.1007/s00429-019-01877-x.

[47] A. Crombe, V. Planche, G. Raffard, J. Bourel, N. Dubourdieu, A. Panatier, T. Tourdias, Deciphering the microstructure of hippocampal subfields with in vivo DTI and NODDI: applications to experimental multiple sclerosis, NeuroImage 172 (2018) 357–368, https://doi.org/10.1016/j.neuroimage.2018.01.061.

[48] K.M. Rodrigue, A.M. Daugherty, C.M. Foster, K.M. Kennedy, Striatal iron content is linked to reduced fronto-striatal brain function under working memory load, NeuroImage 210 (2020), 116544, https://doi.org/10.1016/j.neuroimage.2020.116544.

[49] B. Hallgren, P. Sourander, The effect of age on the non-haemin iron in the human brain, J. Neurochem. 3 (1958) 41–51, https://doi.org/10.1111/j.1471-4159.1958.tb12607.x.

[50] R.D. Badgaiyan, A.J. Fischman, N.M. Alpert, Striatal dopamine release in sequential learning, NeuroImage 38 (2007) 549–556, https://doi.org/10.1016/j.neuroimage.2007.07.052.

[51] A. Rieckmann, H. Fischer, L. Bäckman, Activation in striatum and medial temporal lobe during sequence learning in younger and older adults: relations to performance, NeuroImage 50 (2010) 1303–1312, https://doi.org/10.1016/j.neuroimage.2010.01.015.

[52] C.M. Stillman, E.M. Gordon, J.R. Simon, C.J. Vaidya, D.V. Howard, J.H. Howard, Caudate resting connectivity predicts implicit probabilistic sequence learning, Brain Connect. 3 (2013) 601–610, https://doi.org/10.1089/brain.2013.0169.

[53] K. Janacsek, K.F. Shattuck, K.M. Tagarelli, J.A.G. Lum, P.E. Turkeltaub, M. T. Ullman, Sequence learning in the human brain: a functional neuroanatomical

meta-analysis of serial reaction time studies, NeuroImage 207 (2020), 116387, https://doi.org/10.1016/j.neuroimage.2019.116387.
[54] G.E. Alexander, M.R. DeLong, P.L. Strick, Parallel organization of functionally segregated circuits linking basal ganglia and cortex, Annu. Rev. Neurosci. 9 (1986) 357–381, https://doi.org/10.1146/annurev.ne.09.030186.002041.
[55] Carol A. Seger, The basal ganglia in human learning, Neuroscientist 12 (2006) 285–290, https://doi.org/10.1177/1073858405285632.
[56] E. Langnes, M.H. Sneve, D. Sederevicius, I.K. Amlien, K.B. Walhovd, A.M. Fjell, Anterior and posterior hippocampus macro- and microstructure across the lifespan in relation to memory—a longitudinal study, Hippocampus 30 (2020) 678–692, https://doi.org/10.1002/hipo.23189.
[57] L.S. Morris, P. Kundu, N. Dowell, D.J. Mechelmans, P. Favre, M.A. Irvine, V. Voon, Fronto-striatal organization: defining functional and microstructural substrates of behavioural flexibility, Cortex 74 (2016) 118–133, https://doi.org/10.1016/j.cortex.2015.11.004.